

Pressure-induced amorphization of metavanadate crystals SrV₂O₆ and BaV₂O₆

Yan Li, Ruilian Tang, Nana Li, Hui Li, Xudong Zhao, Pinwen Zhu, and Xin Wang

Citation: *Journal of Applied Physics* **118**, 035902 (2015); doi: 10.1063/1.4926784

View online: <http://dx.doi.org/10.1063/1.4926784>

View Table of Contents: <http://scitation.aip.org/content/aip/journal/jap/118/3?ver=pdfcov>

Published by the [AIP Publishing](#)

Articles you may be interested in

[Pressure-induced amorphization in orthorhombic Ta₂O₅: An intrinsic character of crystal](#)

J. Appl. Phys. **115**, 193512 (2014); 10.1063/1.4879245

[Pressure-induced structural evolution and amorphization in Eu₃Ga₅O₁₂](#)

J. Appl. Phys. **114**, 163521 (2013); 10.1063/1.4827836

[Structural and vibrational properties of phenanthrene under pressure](#)

J. Chem. Phys. **139**, 104302 (2013); 10.1063/1.4820359

[Raman and x-ray diffraction studies of cationic type-I clathrate I₈Sb₈Ge₃₈: Pressure-induced phase transitions and amorphization](#)

J. Appl. Phys. **105**, 043522 (2009); 10.1063/1.3078807

[Raman and x-ray diffraction studies of Ba doped germanium clathrate Ba₈Ge₄₃ at high pressures](#)

J. Appl. Phys. **101**, 063549 (2007); 10.1063/1.2713354

A promotional banner for AIP Applied Physics Reviews. The background is a dark blue gradient with a bright light source on the right, creating a lens flare effect. On the left, there is a small image of a book cover for 'AIP Applied Physics Reviews' featuring a diagram of a crystal structure. The main text 'NEW Special Topic Sections' is in large, white, bold font. Below this, 'NOW ONLINE' is written in yellow, followed by 'Lithium Niobate Properties and Applications: Reviews of Emerging Trends' in white. The AIP Applied Physics Reviews logo is in the bottom right corner.

NEW Special Topic Sections

NOW ONLINE
Lithium Niobate Properties and Applications:
Reviews of Emerging Trends

AIP Applied Physics
Reviews

Pressure-induced amorphization of metavanadate crystals SrV_2O_6 and BaV_2O_6

Yan Li,^{1,2} Ruilian Tang,^{1,3} Nana Li,^{1,3} Hui Li,¹ Xudong Zhao,⁴ Pinwen Zhu,^{1,a)} and Xin Wang^{1,a)}

¹State Key Laboratory of Superhard Materials, Jilin University, Changchun 130012, China

²College of Physics, Jilin University, Changchun 130012, China

³Center for High Pressure Science and Technology Advanced Research, Shanghai 201203, China

⁴State Key Laboratory of Inorganic Synthesis and Preparative Chemistry, Jilin University, Changchun 130012, China

(Received 14 April 2015; accepted 2 July 2015; published online 15 July 2015)

Lattice vibrations and electrical transport properties of SrV_2O_6 (SVO) and BaV_2O_6 (BVO) under high pressure have been investigated by Raman spectra and alternating current (AC) impedance spectra measurements. A pressure-induced structural phase transition in SVO is observed at 3.9 GPa, and the phase transition in BVO happens at 4.3 GPa from their high-pressure Raman spectra. With further increasing pressures, amorphization is found in both SVO and BVO at 10.1 and 9.3 GPa, respectively. Pressure-induced amorphization of SVO and BVO is suggested to be associated with the breaking up of infinite chains of corner-linked tetrahedral VO_4 into VO_3^- . The recovery of original crystalline phases along with the re-linking of VO_3^- chains is observed after heating the reclaimed samples. Furthermore, the *in situ* high pressure measurements of AC impedance spectra of BVO reveal two distinct changes in its resistance, which can correspond to the transitions as observed in the Raman spectra. © 2015 AIP Publishing LLC.

[<http://dx.doi.org/10.1063/1.4926784>]

I. INTRODUCTION

Metavanadate compounds with divalent metal atoms have the general formula of MV_2O_6 ($M = \text{Mg, Ca, Ba, Sr, etc.}$) and adopt structural types consisting of the frameworks of V–O polyhedra together with interstitial M^{2+} ions.¹ These compounds have potential applications as alternative anode of lithium ion rechargeable batteries, which are characterized by their higher discharge capacity, excellent recyclability, thermal stability, low-cost, and environmental benefits.^{2–7} Most of the divalent metal metavanadates crystallize in a brannerite-like structure constituted by the zigzag chains of VO_5 square pyramids with sharing edges, for example, MV_2O_6 with $M = \text{Mg, Mn, Co, and Zn}$ adopts this type of structure.^{8–12} In contrast, SrV_2O_6 (SVO)/ BaV_2O_6 (BVO) with a larger divalent metal atom adopts the structure featured by VO_4 tetrahedral units. This type of structure consists of corner-sharing VO_4 tetrahedra forming infinite chains, which is similar to alkali-metal vanadates MVO_3 ($M = \text{Li, Na, K, etc.}$).^{13–17}

In general, subjecting the materials to extreme conditions can reveal more interesting properties, and high pressure studies of these alkali-metal vanadates, such as MVO_3 ($M = \text{Li, Na, K, etc.}$), $\alpha\text{-NaV}_2\text{O}_5$, and $\beta\text{-Na}_{0.33}\text{V}_2\text{O}_5$, have attracted considerable attentions due to the pressure-induced phase transitions and thus the improved physical properties, which can have efficient effects on their applications.^{18–27} Moreover, MVO_3 ($M = \text{Li, Na, K, etc.}$) belongs

to the pyroxene family, and the studies may be of geophysical interest. From previous high-pressure studies, most of these materials showed structural phase transitions that were believed to be a series of transformations involving the breaking up of infinite VO_4 chains into VO_3^- ions. All these phase transitions were preceded by the changes of chain deformation motions, most probably the variation in V–O–V bond angles as characterized by the measurements of the corresponding vibrational modes. Because of the structural similarities between SVO/BVO and alkali-metal vanadates MVO_3 , possible structural phase transitions are expected from the high-pressure Raman studies on SVO/BVO.

Pressure-induced amorphization (PIA) has been the subject of intense study for the past few years because of its importance in materials science and solid state physics.^{28–30} Thus, another motivation in undertaking the present study of SVO/BVO is to search for possible PIA similar to that reported in NaVO_3 .³¹ The crystalline-amorphous transition of NaVO_3 occurred at 6 GPa, which was the lowest transformation pressure for an amorphous phase so far reported for vanadates.³² PIA in NaVO_3 was identified by the sudden appearance of very broad bands in Raman spectra at high pressures. In its amorphous phase, the chains consisting of corner-sharing VO_4 tetrahedra broke up into individual VO_3 pyramids, and it could revert to the stable ambient-condition phase upon heating. Shear instability was thought to be the cause for PIA in NaVO_3 . There are also some other examples to exhibit that ionic crystals can become amorphous at high pressures.^{33–35}

In the present work, we have carried out Raman spectra and alternating current (AC) impedance spectra measurements

^{a)}Authors to whom correspondence should be addressed. Electronic addresses: zhupw@jlu.edu.cn and xin_wang@jlu.edu.cn.

on SVO and BVO polycrystalline samples at high pressures in order to investigate their structural behaviors and benefit further understanding of the electrical transport properties under high pressure. A structural phase transition for SVO/BVO is observed at 3.9 and 4.3 GPa, respectively, and PIA of SVO/BVO is found to occur at 10.1 and 9.3 GPa, respectively. After releasing the pressure and heating the recovered samples, Raman spectra show that the PIA phase of SVO and BVO can revert to its original ambient phase. Moreover, the observations of a structural phase transition and amorphization of BVO are also accompanied by the changes of its resistance under high pressure. We hope that the present study can be beneficial for better understanding of the mechanism of PIA in this intriguing family of materials and developing more applications under ambient and extreme conditions.

II. EXPERIMENTAL

Samples of SVO/BVO were synthesized by sol-gel method. Analytical grade V_2O_5 (>99.99%), $M(NO_3)_2 \cdot nH_2O$ (>99%) ($M = Sr, Ba$), and oxalic acid ($H_2C_2O_4$) (>99%) were used as the starting materials. The mixed precursor was pressed into a pellet and then heat treated to obtain the final products. The reaction temperatures were chosen to be 773 K/873 K in air over a period of 10 h for SVO/BVO, respectively.

X-ray diffraction (XRD, RIGAKU) with Cu $K\alpha$ radiation ($\lambda = 1.5418 \text{ \AA}$) was used to determine the phase purity of SVO/BVO, and the results are shown in Figure 1. Diamond anvil cell (DAC) was utilized to generate high pressure, and the anvil culet was $400 \mu\text{m}$ in diameter with a bevelled angle of 10° . T301 stainless steel as the gasket was pre-indented to $50 \mu\text{m}$ thickness, and a hole of $120 \mu\text{m}$ in diameter was drilled at the center of the indentation. The powder samples were loaded into DAC with chips of ruby for pressure calibration by ruby luminescence technique.³⁶ A 16:3:1 methanol/ethanol/water mixture was chosen as pressure medium to provide hydrostatic conditions. High-pressure Raman spectra of SVO/BVO over a wavenumber range between 100 and 1200 cm^{-1} were measured at room temperature up to 14.3 and 11.6 GPa, respectively. Raman spectra were recorded on a Renishaw in Via Raman microscope in the backscattering geometry using the 514.5 nm line of an argon ion laser, provided with a charge coupled device (CCD) detector system. Pressure-induced shifts of overlapping Raman bands were analyzed by fitting the spectra to Lorentzian functions to determine the line shape parameters.

Van der Pauw electrodes were integrated on one diamond for the electric properties measurement under pressure. The fabricated process of the detecting microcircuit has been reported in our previous publications.^{37,38} The samples used in the electrical measurement were squeezed into a disk with $120 \mu\text{m}$ in diameter. The measurements of AC impedance spectroscopy were in the frequency range of 1 Hz–10 MHz and the applied alternating current voltage was 1 V.

III. RESULT AND DISCUSSION

The structure of SVO is similar to that of BVO. Both of them crystallize in orthorhombic structure with the space group

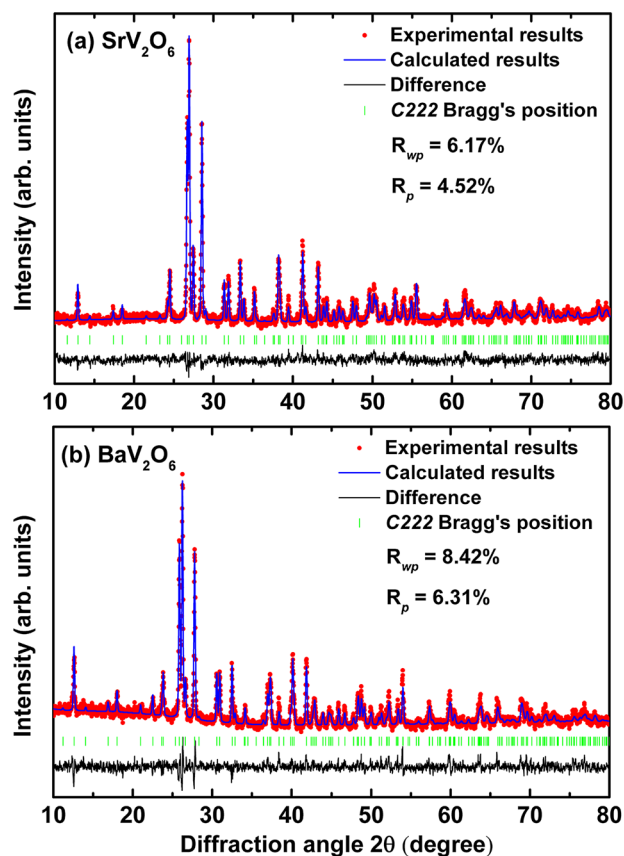


FIG. 1. Rietveld full-profile refinement of the diffraction patterns of (a) SrV_2O_6 and (b) BaV_2O_6 at ambient condition. Red, blue, and black solid lines represent experimental, calculated, and residual patterns, respectively. Vertical markers show the calculated peak positions.

C222 (No. 21) and the refined lattice parameters are followed as $a = 8.245(1) \text{ \AA}$, $b = 12.293(1) \text{ \AA}$, $c = 7.657(2) \text{ \AA}$, $Z = 6$, $V = 776.08 \text{ \AA}^3$ (SVO) and $a = 8.482(1) \text{ \AA}$, $b = 12.611(2) \text{ \AA}$, $c = 7.916(1) \text{ \AA}$, $Z = 6$, $V = 845.17 \text{ \AA}^3$ (BVO). As an example shown in Figure 2, the structure of BVO consists of infinite chains of vertex-shared VO_4 tetrahedra running along the $[120]$ directions and Ba atoms located interstitially between the chains. Ba(1) is coordinated by twelve oxygen atoms and Ba(2) by ten oxygen atoms. The similar structural features also exist in alkali-metal vanadates MVO_3 ($M = Na, K$, etc.), which show a little difference from BVO, the chains of MVO_3 run straight along the orthorhombic a -axis, and the neighbouring zigzag chains are interspersed with each other.³⁹

The Raman spectra of SVO have been measured up to 14.3 GPa, and some selected Raman spectra are shown in Figure 3(a). There are 14 modes clearly observed in a Raman spectrum of SVO at room temperature. Based on the previous Raman experiments of alkali metavanadate MVO_3 with chains of vertex-shared VO_4 tetrahedra, the Raman bands in the spectral region below 400 cm^{-1} were identified to be VO_2 rocking, twisting, and chain deformation vibrations.^{16–18,21–23,31,32} The band at 470 cm^{-1} was assigned to $\delta\text{-}VO_2$, which should be sensitive to the repacking of the lattice or the change of cation coordinated environment and essentially unchanged too much upon compression.³¹ The bands in the region of $500\text{--}800 \text{ cm}^{-1}$ belonged to the

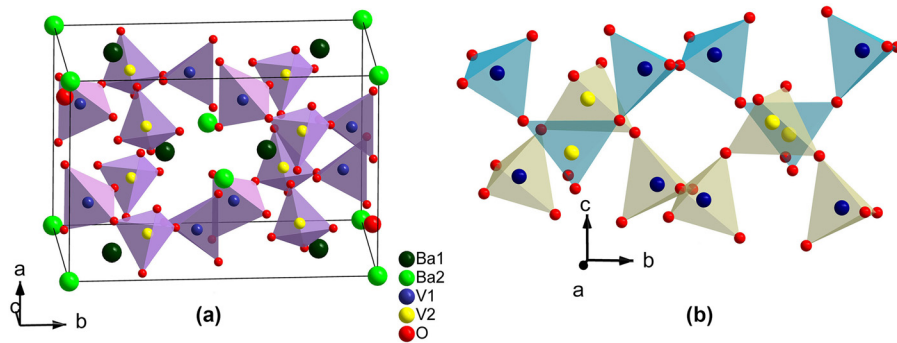


FIG. 2. (a) The crystal structure of BVO and (b) infinite chains formed by shared-corners VO₄ tetrahedra.

vibration of V–O–V symmetric stretching mode, whereas the bands in the region of 800–1000 cm⁻¹ were associated with the vibrations of VO₂.¹⁶

With increasing pressures, all the Raman spectra appear similar below 3.9 GPa. Dramatic spectral changes occur above 3.9 GPa. The peaks of low frequency region (below 400 cm⁻¹) become broadening, as shown in Figure 3(a), and it can be seen that the slopes for the frequency increments are also to increase largely after 3.9 GPa, as shown in Figure 3(b). More interestingly, a set of new peaks (located at 689 cm⁻¹, 723 cm⁻¹, 771 cm⁻¹, and 857 cm⁻¹) suddenly appear, and the intensities of these new peaks increase with increasing pressures. It suggests that a possible structural phase transition takes place at 3.9 GPa. At 8.8 GPa, the band at 771 cm⁻¹ (labeled as A) becomes the most dominant in the entire spectrum. While the original strongest peak at 978 cm⁻¹ reduces a lot as the pressure increases, but it does not completely disappear. The new high-pressure phase labeled as phase II is likely to be a mixture phase since the spectra show a continuous change from 3.9 GPa to 10.1 GPa. With further increasing pressures, most of the sharp bands have disappeared at 10.1 GPa and no Raman peaks can be observed above 12.3 GPa. Upon releasing pressure, the spectrum of the starting orthorhombic phase is not recovered, and only very broad

bands exist, which suggests the formation of an amorphous phase.

From the above high pressure Raman results, it can be seen that the structure of SVO is stable below 3.9 GPa at room temperature. Above 3.9 GPa, the Raman spectra exhibit clear evidence for a structural phase transition. A high-pressure X-ray diffraction experiment is necessary to solve the observed high-pressure phase. However, according to the experimental studies of many vanadium oxide-based compounds that are made up of tetrahedral VO₄ units, we speculate that the peak at 771 cm⁻¹ in phase II can be assigned to individual VO₃⁻ ions rather than broken chains formed by shared-corners VO₄ tetrahedra.^{21,24,40} Nevertheless, there exist small but definite bands around the 900 cm⁻¹ region in phase II, indicating that there are still some broken chains left at pressures up to 10.1 GPa. With increasing pressures, the rapid decrease in the intensity of the 964 cm⁻¹ mode and the appearance of the 771 cm⁻¹ peak, which are the characteristics of V–O–V stretching vibration, strongly support the increased degree of the broken chains. Above 10.1 GPa, the chains have been deformed so much that they are no longer energetically favourable to maintain the chain formation in an infinite way. The excessive broadening of the stretching modes and the increased

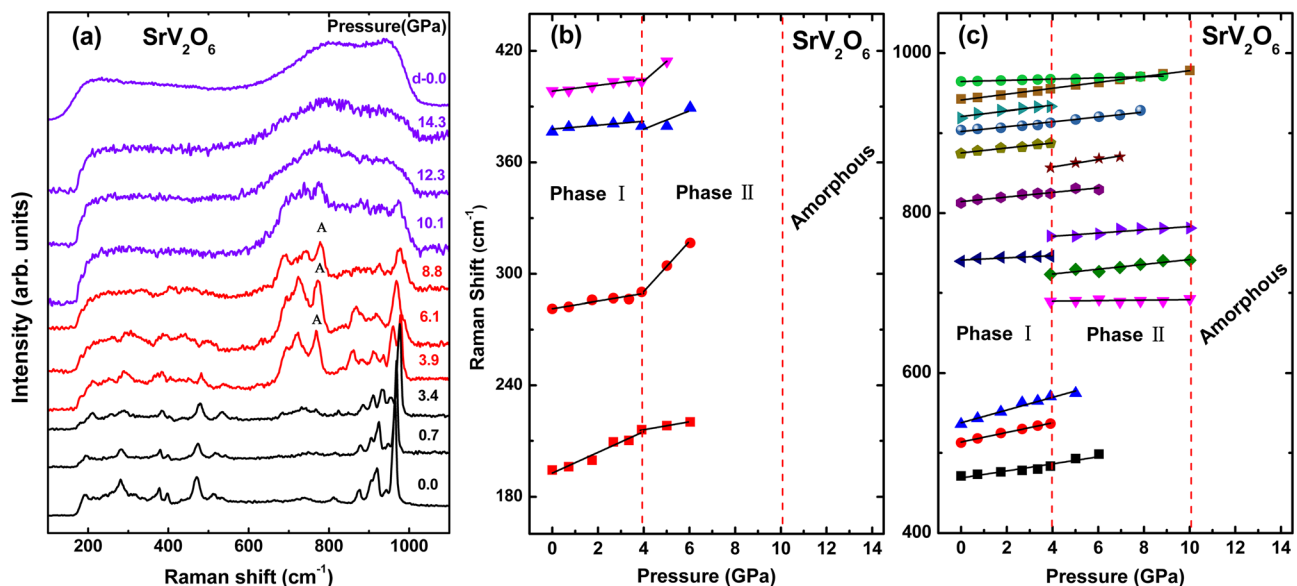


FIG. 3. (a) Representative Raman spectra of SVO at various pressures. (b) Pressure dependence of the Raman frequencies for the bands below 400 cm⁻¹. (c) Pressure dependence of the Raman frequencies for the bands above 400 cm⁻¹. The vertical dashed lines indicate the pressure at which the transition takes place.

background in the mode region of chain deformation suggest that the SVO crystal turns into an amorphous phase. The amorphous phase is speculated to be involved with the complete breaking up of the infinite chains of corner linked tetrahedral VO_4 and most likely into VO_3^- ions above 12.3 GPa, which is similar to the case of MVO_3 .^{21,24,40} Even on releasing the pressure from 14.3 GPa, Raman spectrum does not recover to the original spectrum at ambient condition. It indicates that the process of amorphization is nonreversible.

The ambient spectrum of BVO clearly resembles that of SVO, and the assignments and classifications of the Raman bands can be derived from those of SVO. The high pressure Raman spectra of BVO have been measured up to 11.6 GPa, and some selected Raman scattering spectra are given in Figure 4(a). The Raman bands in the spectra below 400 cm^{-1} are identified to be VO_2 rocking, twisting, and chain deformation vibrations. The band at 466 cm^{-1} is assigned to $\delta\text{-VO}_2$. The band in the region of $500\text{--}880\text{ cm}^{-1}$ belongs to the vibration of V–O–V symmetric stretching mode. The bands in the region of $880\text{--}1000\text{ cm}^{-1}$ are associated with the vibrations of VO_2 .

As can be seen in Figure 4(a), the spectra do not show any obvious changes below 4.3 GPa. Beyond that, some new peaks come up suddenly (located at 806 cm^{-1} , 840 cm^{-1} , and 873 cm^{-1}). The process of phase transition is similar to SVO as discussed above. The Raman shifts of both ambient phase and high-pressure phase as a function of pressure are presented in Figure 4(b). Upon compression, the smeared bands around $500\text{--}880\text{ cm}^{-1}$ suggest that VO_4 chains are partially broken at 4.3 GPa, and with further increasing pressure, the degree of broken chains is also increasing. Finally, BVO turns into completely amorphous at 9.3 GPa. The mechanism of PIA is also attributed to the complete breaking up of infinite chains of these corner-linked tetrahedral VO_4 and most likely into VO_3^- ions as the same for SVO.

After releasing the pressure, PIA of SVO/BVO is maintained, which indicates the nonreversible nature of the phase transitions. However, it had been reported that NaVO_3 and

LiVO_3 were the typical PIA materials, and the Raman spectra of them could revert to their original phase after heating to 623 and 723 K, respectively.^{24,32} Therefore, the same treatment on SVO/BVO is adopted, and the PIA phase of SVO/BVO is heated in an oven in order to examine the recrystallized process. It is apparent that there is sufficient thermal energy at 623 K for individual VO_3^- ions to relink themselves into infinite VO_4 chains and form “perfect” crystals again. The recorded spectrum after heating is almost identical to that of the original phase of SVO/BVO, as shown in Figure 5.

It has been demonstrated in many cases that the abnormal change of structure consequentially brings some influences on the electrical transport coefficient, such as the structural phase transition of CdS under high pressure accompanied by an obvious change in its impedance spectroscopy.⁴¹ Hence, we have measured the AC impedance spectroscopy of SVO and BVO at high pressures in order to extract more information of pressure effects on these two samples. Because SVO is a very good insulator at ambient condition and the value of its resistance reaches out of the limit of our experimental instruments, we cannot obtain its resistance data during the impedance spectroscopy measurement at high pressures. For BVO, the impedance data obtained at different pressures are presented in Figures 6(a)–6(c). The diameter of the arc becomes smaller and smaller with the pressure increased up to 3.7 GPa, but the situation is reversed above 3.7 GPa.

In order to quantify the pressure effect on the electrical transport properties of BVO, the impedance spectra data are fitted with an equivalent circuit consisting of resistor (R) and constant phase element (CPE) by using the Zview impedance analysis software (version 2.7, Scribner Associates Inc.) as shown in Figure 6(d). The values of the resistance are directly obtained from the fitting results, as shown in Figure 7. At the beginning, the resistance of BVO shows a rapid decrease with the pressure increased up to 3.7 GPa and then it exhibits a smooth and slow decrease in the pressure range from

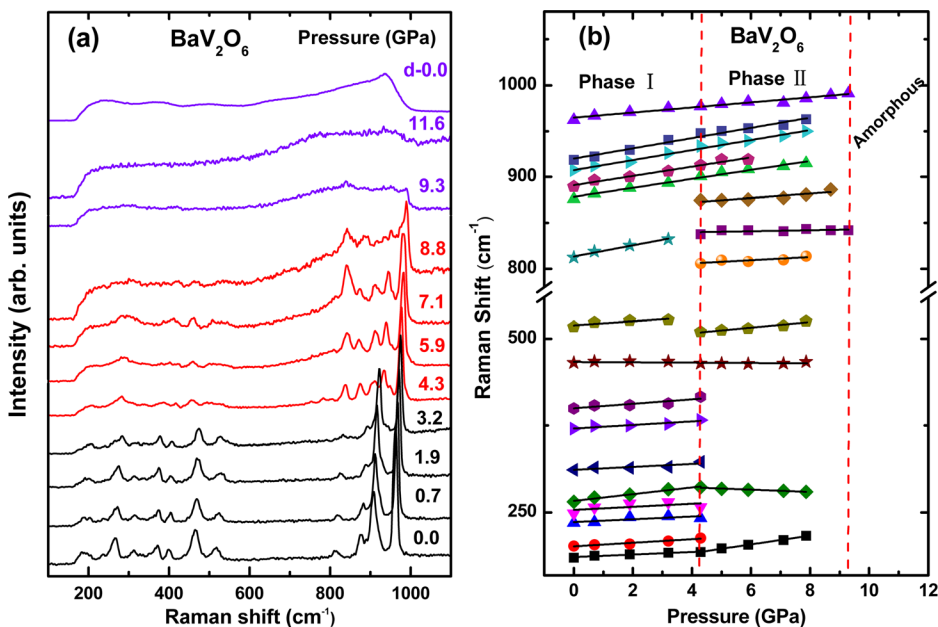


FIG. 4. (a) The evolution of Raman spectra of BVO at high pressures. (b) Pressure dependence of the shifts of Raman active modes for BVO. The vertical dashed lines indicate the pressure at which the transition takes place.

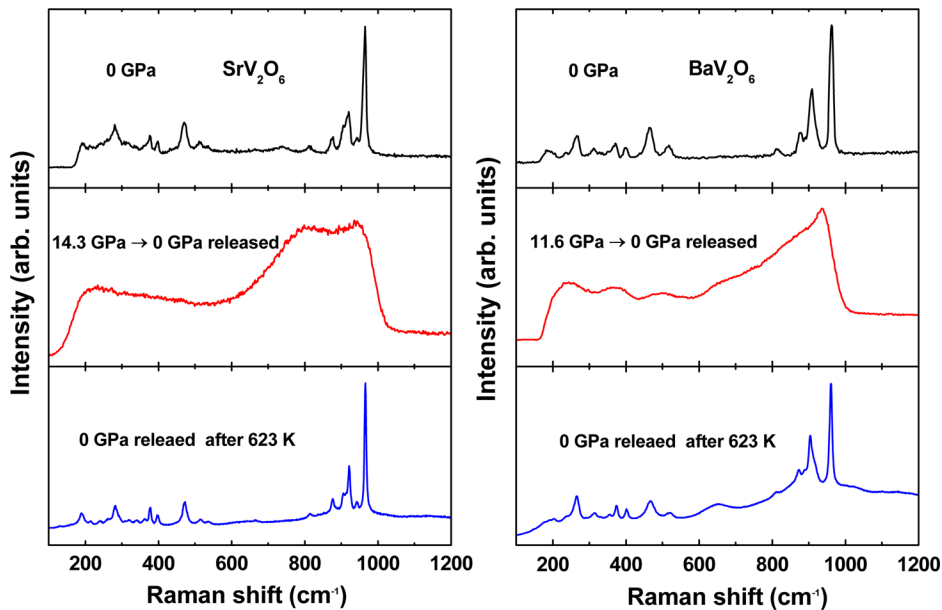


FIG. 5. The crystalline original phase of SVO/BVO is restored after heating the samples at 623 K, which is indicated by the sharp bands in the corresponding spectrum.

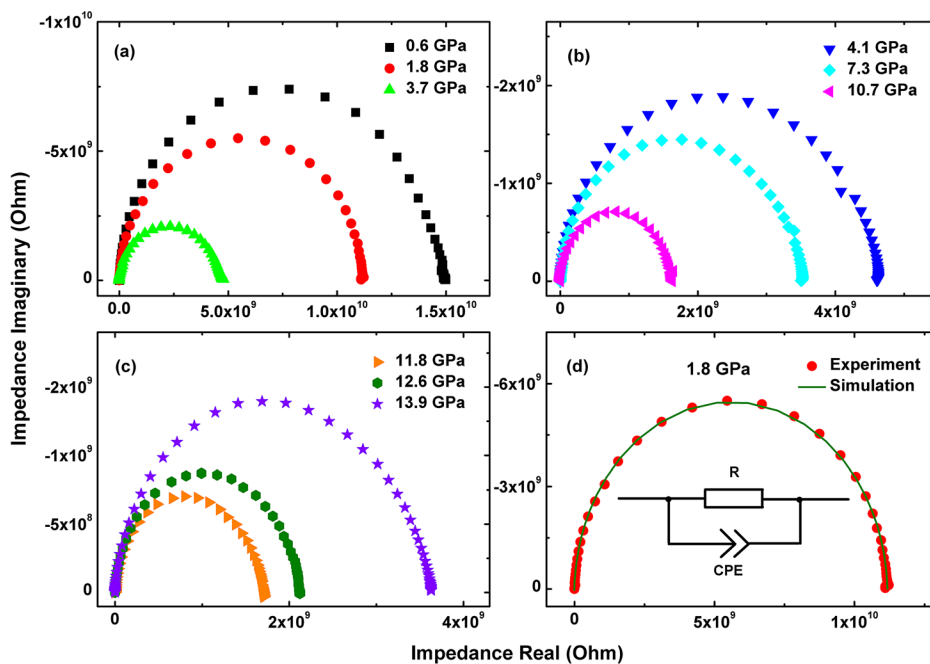


FIG. 6. (a)–(c) The Nyquist plots of impedance spectroscopy of BaV_2O_6 at different pressures. The AC impedance spectroscopy is measured in the frequency range of 1 Hz–10 MHz. (d) Equivalent circuit is used to represent the electrical properties of BaV_2O_6 at 1.8 GPa.

3.7 GPa to 10.7 GPa. In general, the valence bands and conduction bands of a typical ionic solid tend to become broad with increasing pressures. Since both valence band maximum and conduction band minimum move toward the Fermi level gradually, it will result in the reduction of the band gap. So, the resistance of the material decreases with pressure increased in the crystalline phase. After 10.7 GPa, the resistance shows an increase with increasing pressures. When the sample becomes amorphous under pressure, the crystal lattice will be reconstructed and the scattering effect of the carriers from the grain boundary will be enhanced. It will result in an increase of the resistance in the amorphous phase of the sample. These two pronounced discontinuous kinks of resistance can correspond to the abnormal changes in the above high pressure Raman spectra and clearly provide a further proof that BVO undergoes a phase transition near 4 GPa and a pressure-induced amorphization near 11 GPa.

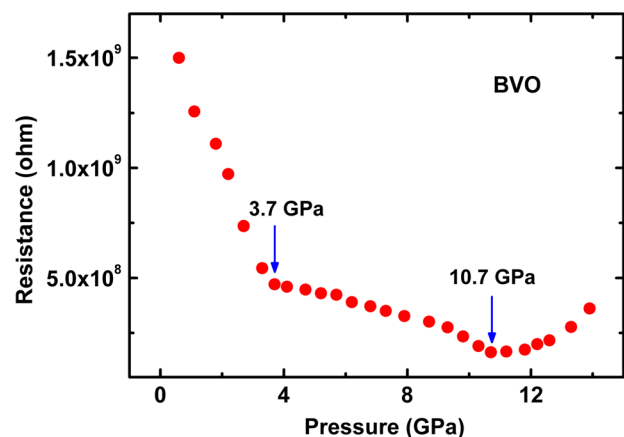


FIG. 7. The fitting result of the resistance of BaV_2O_6 versus pressure.

IV. CONCLUSION

In the present work, the structural and electrical transport properties of SVO/BVO at high pressures have been studied with Raman spectra and AC impedance spectra. A pressure-induced structural phase transition in SVO is observed at 3.9 GPa, and the same phase transition happens in BVO at 4.3 GPa. Our Raman experimental results indicate that PIA of SVO/BVO is found to occur at 10.1 and 9.3 GPa, respectively. The transformation of PIA is involved with the tetrahedral VO₄ chains breaking up abruptly at the transition pressure. After releasing the pressure, the amorphous structure does not have enough energy to rearrange itself into a crystalline structure and instead it remains the amorphous phase. However, by given enough thermal energy, these amorphous phases of SVO/BVO can revert to their ambient phases after heating the reclaimed samples at 623 K. Meanwhile, the structural phase transition and PIA of BVO are also observed to be accompanied by the sudden changes of its resistance at high pressures. These results should be helpful for better understanding of the physical properties in this type of materials.

ACKNOWLEDGMENTS

This work was financially supported by the National Natural Science Foundation of China under Grant No. 51172091, the Program for New Century Excellent Talents in University, China (NCET-12-0240), Jilin Province Science and Technology Development Program, China (20130101023JC), and the Open Project of State Key Laboratory of Superhard Materials (Jilin University).

¹K. Waltersson, *Chem. Commun. (Univ. Stockholm)* **7**, 83 (1976).

²E. Andrukaitis, J. P. Cooper, and J. H. Smit, *J. Power Sources* **54**, 465 (1995).

³X. Cao, J. Xie, H. Zhan, and Y. Zhou, *Mater. Chem. Phys.* **98**, 71 (2006).

⁴S. Ni, G. Zhou, X. Wang, X. Sun, F. Yang, Y. Liu, and D. He, *Mater. Chem. Phys.* **120**, 426 (2010).

⁵J. Q. Cao, X. Y. Wang, A. Tang, and X. Wang, *J. Alloys Compd.* **479**, 875 (2009).

⁶A. A. Belik, A. V. Mironov, R. V. Shpanchenko, and E. Takayama-Muromachi, *Acta Crystallogr., Sect. C: Cryst. Struct. Commun.* **63**, i37 (2007).

⁷H. Fang, Z. C. Hua, S. Zhang, M. Xing, C. Gang, W. V. Jin, and W. C. Zhong, *Chem. Res. Chin. Univ.* **27**, 528 (2011).

⁸H. N. Ng and C. Calvo, *Can. J. Chem.* **50**, 3619 (1972).

⁹R. Kozłowski, J. Ziółkowski, K. Mocała, and J. Haber, *J. Solid State Chem.* **35**, 1 (1980).

¹⁰K. Mocała, J. Ziółkowski, and L. Dziembaj, *J. Solid State Chem.* **56**, 84 (1985).

¹¹H. Liu and D. Tang, *Mater. Chem. Phys.* **114**, 656 (2009).

¹²R. Ruh and A. D. Wadsley, *Acta Crystallogr.* **21**, 974 (1966).

¹³H. T. Evans, Jr., *Z. Kristallogr.* **114**, 257 (1960).

¹⁴M. Ganne, Y. Piffard, and M. Tournoux, *Can. J. Chem.* **52**, 3539 (1974).

¹⁵F. Hawthorne and C. Calvo, *J. Solid State Chem.* **22**, 157 (1977).

¹⁶S. Seetharaman, H. L. Bhat, and P. S. Narayanan, *J. Raman Spectrosc.* **14**, 401 (1983).

¹⁷A. Grzechnik and P. F. McMillan, *J. Phys. Chem. Solids* **56**, 159 (1995).

¹⁸D. M. Adams and P. A. Fletcher, *Spectrochim. Acta, Part A* **44**, 233 (1988).

¹⁹D. M. Adams, A. G. Christy, J. Haines, and S. Leonard, *J. Phys.: Condens. Matter* **3**, 6135 (1991).

²⁰D. M. Adams, J. Haines, and S. Leonard, *J. Phys.: Condens. Matter* **3**, 2859 (1991).

²¹G. Kourouklis, A. Jayaraman, G. Espinosa, and A. Cooper, *J. Raman Spectrosc.* **22**, 57 (1991).

²²Z. X. Shen, C. W. Ong, S. H. Tang, and M. H. Kuok, *J. Phys. Chem. Solids* **55**, 661 (1994).

²³S. H. Tang, M. H. Kuok, Z. X. Shen, and C. W. Ong, *J. Phys.: Condens. Matter* **6**, 6565 (1994).

²⁴Z. X. Shen, C. W. Ong, M. H. Kuok, and S. H. Tang, *J. Phys.: Condens. Matter* **7**, 939 (1995).

²⁵R. K. Kremer, I. Loa, F. S. Razavi, and K. Syassen, *Solid State Commun.* **113**, 217 (1999).

²⁶T. Yamauchi, Y. Ueda, and N. Mori, *Phys. Rev. Lett.* **89**, 057002 (2002).

²⁷C. A. Kuntscher, S. Frank, I. Loa, K. Syassen, T. Yamauchi, and Y. Ueda, *Phys. Rev. B* **71**, 220502 (2005).

²⁸E. G. Ponyatovsky and O. I. Barkalov, *Mater. Sci. Rep.* **8**, 147 (1992).

²⁹A. V. Kolobov, J. Haines, A. Pradel, M. Ribes, P. Fons, J. Tominaga, C. Steimer, G. Aquilanti, and S. Pascarelli, *Appl. Phys. Lett.* **91**, 021911 (2007).

³⁰X. Q. Yan, W. J. Li, T. Goto, and M. W. Chen, *Appl. Phys. Lett.* **88**, 131905 (2006).

³¹Z. X. Shen, C. W. Ong, S. H. Tang, and M. H. Kuok, *Phys. Rev. B* **49**, 1433 (1994).

³²Z. X. Shen, C. W. Ong, S. H. Tang, and M. H. Kuok, *J. Phys. Chem. Solids* **55**, 665 (1994).

³³C. A. Perottoni and J. A. H. da Jornada, *Science* **280**, 886 (1998).

³⁴T. Varga, A. P. Wilkinson, C. Lind, W. A. Bassett, and C. S. Zha, *Solid State Commun.* **135**, 739 (2005).

³⁵T. Sakuntala, A. K. Arora, V. Sivasubramanian, R. Rao, S. Kalavathi, and S. K. Deb, *Phys. Rev. B* **75**, 174119 (2007).

³⁶H. K. Mao, P. Bell, J. W. Shaner, and D. Steinberg, *J. Appl. Phys.* **49**, 3276 (1978).

³⁷Y. H. Han, C. X. Gao, Y. Z. Ma, H. W. Liu, Y. W. Pan, J. F. Luo, M. Li, C. Y. He, X. W. Huang, and G. T. Zou, *Appl. Phys. Lett.* **86**, 064104 (2005).

³⁸M. Li, J. Yang, K. Snoussi, L. X. Li, H. X. Wang, and C. X. Gao, *Appl. Phys. Lett.* **97**, 174101 (2010).

³⁹T. Yao, Y. Oka, and N. Yamamoto, *Inorg. Chim. Acta* **238**, 165 (1995).

⁴⁰A. M. Heyns, M. W. Venter, and K.-J. Range, *Z. Naturforsch. B: Chem. Sci.* **42**, 843 (1987).

⁴¹C. Y. He, C. X. Gao, Y. Z. Ma, M. Li, A. M. Hao, X. W. Huang, B. Liu, D. M. Zhang, C. L. Yu, and G. T. Zou, *Appl. Phys. Lett.* **91**, 092124 (2007).